

Rupture of thin liquid films on structured surfacesVladimir S. Ajaev¹¹*Department of Mathematics, Southern Methodist University, Dallas, Texas 75275, USA*Elizaveta Ya. Gatapova^{2,3} and Oleg A. Kabov^{2,3,4}²*Institute of Thermophysics, SB RAS Novosibirsk 630090, Russia*³*Microgravity Research Center, Department of Chemical Physics, Universite Libre de Bruxelles, C. P. 165/62, B-1050 Brussels, Belgium*⁴*Center of Smart Interfaces, Technische Universitaet Darmstadt, D-64287 Darmstadt, Germany*

(Received 30 August 2010; published 28 October 2011)

We investigate stability and breakup of a thin liquid film on a solid surface under the action of disjoining pressure. The solid surface is structured by parallel grooves. Air is trapped in the grooves under the liquid film. Our mathematical model takes into account the effect of slip due to the presence of menisci separating the liquid film from the air inside the grooves, the deformation of these menisci due to local variations of pressure in the liquid film, and nonuniformities of the Hamaker constant which measures the strength of disjoining pressure. Both linear stability and strongly nonlinear evolution of the film are analyzed. Surface structuring results in decrease of the fastest growing instability wavelength and the rupture time. It is shown that a simplified description of film dynamics based on the standard formula for effective slip leads to significant deviations from the behavior seen in our simulations. Self-similar decay over several orders of magnitude of the film thickness near the rupture point is observed. We also show that the presence of the grooves can lead to instability in otherwise stable films if the relative groove width is above a critical value, found as a function of disjoining pressure parameters.

DOI: [10.1103/PhysRevE.84.041606](https://doi.org/10.1103/PhysRevE.84.041606)

PACS number(s): 68.15.+e

I. INTRODUCTION

Microfluidic devices incorporating structured surfaces have a potential for significant improvement of liquid transport due to slip reduction observed when gas is trapped between the elements of the structure [1]. However, mathematical models motivated by such applications usually focus on behavior of single-phase flows near structured surfaces [2,3]. In practical microfluidic applications, the flow is often multiphase, with bubbles, droplets, or biological cells transported through networks of microchannels [4,5]. Modeling the behavior of fluid interfaces near structured surface is crucial for development of these applications. One obvious example is a situation when a liquid film separating a moving bubble or droplet from the wall breaks up, possibly resulting in significant reduction of transport rate. Structured surfaces are also used in a variety of heat transfer devices for intensification of single-phase and two-phase heat transfer [6,7]. Liquid film rupture in these applications can have a significant influence on heat transfer rates. The minimum heat flux required for rupture of a gravity-driven liquid film on a grooved plate was recently studied experimentally by Zaitsev *et al.* [7]. As liquid evaporates, the film eventually thins to the point where rupture can occur, and the rupture conditions clearly depend on the parameters of the structuring. Determining these conditions is an important step in the development of novel microscale systems for cooling of electronic devices [8,9].

The issue of fluid interface interaction with a structured surface received little attention in the literature, except for the special case of a liquid droplet bouncing off or rolling on a superhydrophobic surface [10]. In the present study we address this issue in a setting relevant for microfluidic applications by examining the conditions of rupture of a thin liquid film between a gas-liquid interface and a grooved surface with gas

trapped in the grooves. The film is assumed to be thin enough so that the rupture is driven by the London–van der Waals dispersion forces.

The general framework for mathematical modeling of thin film rupture under the action of the London–van der Waals forces was developed in the pioneering works of Williams and Davis [11] and Burelbach *et al.* [12] in the context of liquid films on flat and chemically homogeneous solid substrates. They used a lubrication-type model of the viscous flow in the film and carried out numerical simulations of the resulting evolution equation for film thickness. Zhang and Lister [13] extended the lubrication-type approach to axisymmetric geometry and found self-similar solutions which incorporate the effects of London–van der Waals forces, viscous dissipation, and surface tension for both two-dimensional and axisymmetric rupture. The linear and nonlinear stability and rupture time of ultrathin fluid films on coated nonwettable substrates were studied by Khanna *et al.* [14]. They found that the film breakup time is sensitive to the coating properties even for relatively thick films.

The effect of the chemical heterogeneity of the substrate on the dewetting in a thin liquid film was considered by Thiele *et al.* [15], Sharma *et al.* [16], and Kao *et al.* [17]. These authors investigated how pattern formation in the dewetting liquid film depends on the parameters of the heterogeneity. In particular, Thiele *et al.* [15] identified the conditions when the solid substrate pattern is transferred onto the liquid film structure. For a substrate pattern of alternating stripes of different wettability, Sharma *et al.* [16] showed that film rupture is suppressed on some potentially destabilizing nonwettable sites when their spacing is below a characteristic lengthscale of instability. Kao *et al.* [17] used weakly nonlinear analysis to investigate the structure of the bifurcation for the liquid film shapes on a solid with periodic sinusoidal or square-wave

patterning and conducted numerical simulations of the film evolution for these two models of chemical heterogeneity.

Limitations of the classical no-slip condition at solid-liquid interfaces, especially for cases when the solid surface is structured, have been discussed in Lauga *et al.* [18]. This review article and more recent studies, e.g. [19], discuss generalized slip boundary condition and methods for calculating the effective slip length. The effects of slippage on the stability, dynamics, and morphology of thin films on solid surfaces from no-slip to moderate slip and to the case of strong slip are analyzed in Kargupta *et al.* [20]. It was shown that a decrease in film thickness causes transitions from weak to moderate- to strong-slip regime. For the case of strong slippage the holes in the film are produced faster, are fewer in numbers, and have less developed rims. Peschka *et al.* [21] considered a strong-slip regime for small Reynolds numbers where van der Waals forces and viscosity are the dominant physical effects. The existence of self-similar solutions was shown and the convergence to these solutions was studied. The presence of the nanobubbles on hydrophobic substrates can have a significant effect on thin film rupture [22]. Bubbles relax the no-slip condition at parts of the lower boundary of the film and modify expressions for disjoining pressure. In the context of heat transfer applications, Gatapova and Kabov [23] examined the effect of slip at the solid-liquid surface for thin liquid film driven by vapor flow in microchannel with a heater at the bottom wall.

The studies of the effects of substrate heterogeneity on film rupture ([15–17]) and the models of slip flow in thin films ([20–23]) represent two mostly independent directions of research in thin film dynamics. In the configuration of interest for the present paper, both the periodic heterogeneity (due to surface structuring) and slip effects (due to the liquid-gas menisci in the grooves) are present and are in fact considered simultaneously, which was not done in the previous studies. In particular, we investigate coupling between the flow and deformation of the menisci separating air in the grooves and the liquid. Such coupling has not been fully understood except for some simple steady flows [2,3,19]. In our study, the deformations of the menisci are both time dependent and spatially nonuniform (in the sense that the deformation amplitudes are different in different grooves).

II. EVOLUTION EQUATION

We consider a film of incompressible Newtonian liquid of density ρ and viscosity μ on a structured surface as sketched in Fig. 1. The grooves of the surface are filled with air so that the liquid does not enter the grooves. The Cartesian coordinates x and y in our two-dimensional model are scaled by d^2/l_m and d , respectively, where d is the characteristic initial thickness of the film and $l_m = (3|A^*|/\sigma)^{1/2}$ is defined in terms of the value A^* of the Hamaker constant for the liquid film on a flat solid substrate and the surface tension σ . At the bottom, the liquid film is bounded by the line $y = h_1(x, t)$ which consists of straight segments corresponding to the solid and the deformable segments corresponding to air-liquid menisci; time is scaled by $\sigma\mu d^5/(3A^{*2})$. The choices of the time scale and the horizontal length scale are motivated by the dimensional dispersion relation from the

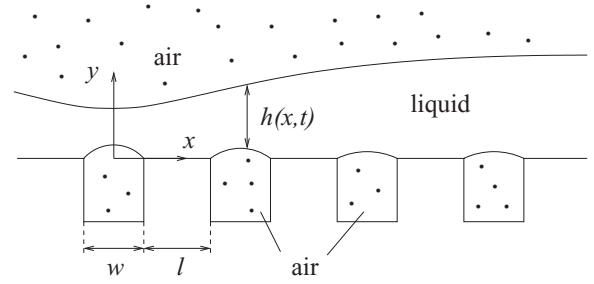


FIG. 1. Sketch of a liquid film on a structured surface and Cartesian coordinates.

linear stability theory of film rupture on flat solid surfaces, as discussed in, for example, Ref. [13]. Even though we expect the instability growth rate and its characteristic wavelength to be affected by the presence of the grooves, our simulations below indicate that these changes are not dramatic enough to justify the use of time and length scales which are different from the case of the flat substrate. We assume the dimensional width of the grooves to be of the same order as d^2/l_m , which is reasonable for microscale structuring; nondimensional groove width is denoted by w and distance between grooves by l . The upper surface of the film is defined by the function $y = h_2(x, t)$.

Let us first consider a region of the film above a groove, so that both $h_1(x, t)$ and $h_2(x, t)$ represent segments of liquid-air interfaces. Using the standard small-slope approximation for the shapes of both interfaces, we write the normal stress conditions in the form,

$$p + \Pi = p_g + h_{1xx} \quad \text{at } y = h_1(x, t), \quad (1)$$

$$p + \Pi = -h_{2xx} \quad \text{at } y = h_2(x, t). \quad (2)$$

Here p is the pressure in the liquid relative to the atmospheric pressure and Π is the disjoining pressure (specified below), both scaled by $3A^*/d^3$. The scaled difference between the air pressure in the groove and the atmospheric pressure, $p_g(t)$, can be a function of time depending on the flow pattern inside the groove, but possible spatial variation of this quantity along the meniscus is neglected. Assuming flow in the liquid is governed by the standard lubrication-type equations under the conditions of negligible gravity, the pressure p is not a function of y [24]. By combining Eqs. (1) and (2), we obtain

$$p = \frac{1}{2}(p_g - h_{xx}) - \Pi. \quad (3)$$

Here we express the pressure in terms of the film thickness defined by $h = h_2 - h_1$. For the portion of the liquid film above the solid segment of the lower boundary, the usual expression for pressure applies:

$$p = -h_{xx} - \Pi. \quad (4)$$

There are transition regions at the edges of the grooves in which neither (3) nor (4) applies and the assumptions of the lubrication theory break down locally. However, it has been established based on both theoretical considerations and comparisons with numerical simulations [25,26] that the lubrication theory still gives accurate predictions of the interface shape when such localized breakdown happens. For

numerical reasons, the transition region can be described using a smoothing function $f(x)$ which varies from 1 above the groove to zero above the solid segment of the interface, so that the pressure gradient driving the flow is expressed as

$$p_x = -\left[\left(1 - \frac{1}{2}f(x)\right)h_{xx} + \Pi\right]_x. \quad (5)$$

To define $f(x)$ we start by introducing a function $S(x)$ such that it is equal to unity everywhere above each groove and equal to zero for the solid segments. The function $f(x)$ is a smooth version of $S(x)$, which according to [27] can be defined by

$$f(x) = \int_{-\infty}^{\infty} S(\tilde{x})\omega_\varepsilon(x - \tilde{x})d\tilde{x}, \quad (6)$$

where the function

$$\omega_\varepsilon(x) = \begin{cases} C_\varepsilon e^{-\varepsilon^2/(\varepsilon^2 - x^2)}, & |x| \leq \varepsilon \\ 0, & |x| > \varepsilon \end{cases} \quad (7)$$

is infinitely differentiable everywhere and identically equal to zero outside of the interval bounded by $x \pm \varepsilon$; ε is a small parameter not exceeding 10^{-2} in all our simulations. The constant C_ε is chosen so that the integral of ω_ε is equal to unity.

The same smoothing function approach is used to account for slip length variations along the surface structure. The scaled slip length,

$$\beta = \beta_0 f(x), \quad (8)$$

is the quantity used in the slip condition at the lower boundary of the film,

$$u = \beta u_y \quad \text{at} \quad y = h_1(x, t). \quad (9)$$

Finite value of the slip at the menisci is due to non-negligible effects of air viscosity at the small scales of the grooves. In principle, the value of β_0 can be determined from the solution of a coupled problem of liquid and air flow, assuming that the grooves are not small enough to be in the Knudsen regime considered by de Gennes [28]. However, in the present work we follow previous studies [3,22] and consider β_0 to be a parameter of the formulation.

The dimensional Hamaker constant in the film above the grooves, A_g^* , can be different from the value of A^* corresponding to the film on a flat solid surface. To take this into account, we write the formula for the disjoining pressure $\Pi(h, x)$ as

$$\Pi(h, x) = -\frac{s + (A_g - s)f(x)}{3h^3}, \quad (10)$$

where $s = A^*/|A^*|$, $A_g = A_g^*/|A_g^*|$. The film thickness is assumed to be much smaller than the depth of the grooves, so that A_g^* is the same as the Hamaker constant for free liquid films and is independent of the groove dimensions.

The lubrication-type velocity profile which satisfies the zero shear stress condition at $y = h_2(x, t)$ and the condition (9) is given by

$$u = \frac{3}{2}p_x[(y - h_2)^2 - h^2] - 3\beta p_x h. \quad (11)$$

Substitution of this velocity profile together with (5) into the integral mass balance condition results in an evolution equation for film thickness,

$$h_t + \left[(h^3 + 3\beta_0 f(x)h^2) \left(\left(1 - \frac{1}{2}f(x)\right)h_{xx} + \Pi(h, x) \right) \right]_x = 0, \quad (12)$$

where $\Pi(h, x)$ is defined by (10). An important special case of $s = A_g = 1$, discussed in detail in the next section, corresponds to the situation when variations of the Hamaker constant due to the presence of the grooves are neglected. This approximation allows us to focus on the physical effects of slip and flow-induced deformation of the menisci separating air in the grooves from the liquid film. The variations of the Hamaker constant are then incorporated into the model in Sec. IV.

III. SOLUTIONS FOR UNIFORM HAMAKER CONSTANT

A. Linear stability

We start by considering Eq. (12) with the disjoining pressure given by

$$\Pi(h, x) = -\frac{1}{3h^3}. \quad (13)$$

The uniform thickness film, $h = 1$, is a solution of (12) with this approximation for disjoining pressure. Let us now investigate its stability with respect to small perturbations $\zeta(x, t) = h(x, t) - 1$, using the linearized version of the evolution equation,

$$\zeta_t + \left[(1 + 3\beta_0 f(x)) \left(\zeta_{xxx} + \zeta_x - \frac{1}{2}f(x)\zeta_{xxx} - \frac{1}{2}f'(x)\zeta_{xx} \right) \right]_x = 0. \quad (14)$$

In the limit of flat substrate ($f(x) = 0$), considering $\zeta \sim e^{\gamma t + ikx}$ results in the well-known analytical dispersion relation [13],

$$\gamma(k) = k^2 - k^4. \quad (15)$$

For the choice of $f(x)$ given by (6), the coefficients of the linearized equation are functions of x , so there is no analytical dispersion relation and the problem has to be solved numerically. Writing $\zeta = e^{\gamma t} \hat{\zeta}(x)$ leads to an eigenvalue problem,

$$\gamma \hat{\zeta} = -\left[(1 + 3\beta_0 f) \left(\hat{\zeta}''' + \hat{\zeta}' - \frac{1}{2}f \hat{\zeta}''' - \frac{1}{2}f' \hat{\zeta}'' \right) \right]', \quad (16)$$

which was solved numerically for the computational domain of length L_c using finite difference discretization with a uniform mesh. For each mesh point i , the derivative of the expression in the square bracket on the right-hand side of (16) is approximated as the difference between its values at half-points of the mesh, $i \pm 1/2$, divided by the mesh size Δx . The condition of zero derivatives at the endpoints was used to define the ghost points outside the computational domain, as needed for the calculation of the derivatives near the endpoints.

It is important to note that each eigenfunction defined by (16) is not a simple sinusoidal function. However, we found that each of them can be represented as a superposition of a leading sinusoidal term of a wave number k and small corrections due to the effects of the structure. We refer to the value of k as the wave number of the perturbation and

order the eigenfunctions by the value of k , which allows us to define the growth rate γ as a function of the wave number.

The size of the computational domain L_c has to be chosen large enough to capture film dynamics. It is important to emphasize that the wave numbers of the perturbations appearing on the surface of flat film are not dictated by the period of the structure; they only depend on the total horizontal extent of the film L_T (determined by the size of the experimental apparatus) and can take virtually any value for sufficiently large L_T . It may seem that solving the problem on the computational domain of size L_c restricts the applicability of the results to systems of size L_c , possibly much smaller than the actual size L_T . However, we found that choosing a computational domain of size $L_c = N_g(w + l)$ with a moderate integer N_g allows us to accurately determine the dispersion relation and, most importantly, find the fastest growing wavelength of the instability. To justify our approach, let us discuss the results of the following computations. First, we carry out the computation on the domain $L_c = N_g(w + l)$ with the number of grooves $N_g = 15$, $w = l = 1$. The conditions of zero derivatives applied at the endpoints dictate the discrete set of wave numbers allowed in the spectrum of the free surface perturbation. The growth rates for these wave numbers, obtained numerically based on (16) with $\beta_0 = 10$, are shown by solid squares in Fig. 2. The solid line is the result of cubic interpolation from the data shown by the squares. Next, we carry out simulations on a larger domain $L_T = 38$, which allows us to sample more perturbation wave numbers; the result is shown by circles. Clearly, the agreement between the actual and the interpolated growth rates on L_T is excellent even for the relatively small number of data points used in the interpolation procedure. The results on the fastest growing instability mode presented below are based on simulations with the domain size $L_c = 30$.

The dashed line in Fig. 2 shows the result of the classical stability analysis for flat substrate, which in our scaled

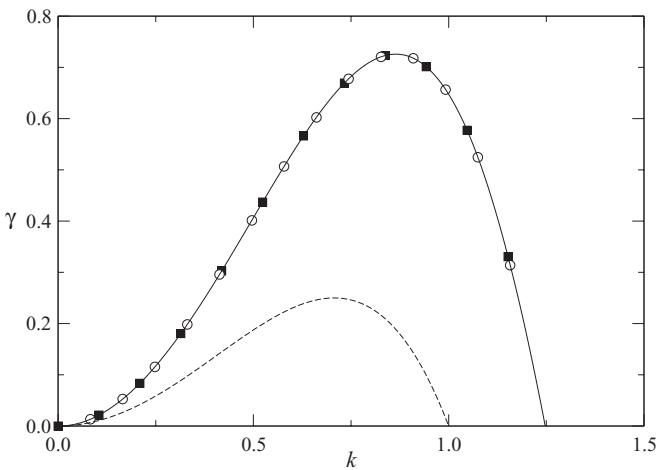


FIG. 2. Numerical dispersion curves obtained based on cubic interpolation from the results on a domain $L_c = 30$ (solid line, with the actual data shown by solid squares) and the data obtained from the simulations with a larger domain size $L_T = 38$ (circles). The parameters are $\beta_0 = 10$, $w = l = 1$, $\varepsilon = 0.01$. Dashed line represents the analytical result for the flat uniform substrate Eq. (15).

variables is represented by (15). Comparing our numerical results with this line, we immediately observe that the surface structuring has a destabilizing effect on the film and also that the fastest growing wavelength λ^* is decreased [since the value of k corresponding to the maximum of $\gamma(k)$ in Fig. 2 is clearly increased]. Let us discuss the physical interpretation of these results. The model of this section incorporates *two* different physical effects related to the presence of the grooves: the appearance of slip region and deformation of the groove meniscii as the flow in the film develops. Addition of slip is clearly destabilizing as it makes it easier for the viscous flow to develop. The effect of having two deforming interfaces is less obvious but it turns out to speed up the development of the instability since it effectively reduces the surface tension (note the $1/2$ factor in front of the nondimensional curvature in the formula for the pressure, Eq. (3)). This has to do with the fact that the capillary pressure jump is calculated from the deformation of the actual interface [e.g., $h_2(x, t)$], and not the change in film thickness $h(x, t)$, which includes contributions from both interfaces and therefore overestimates the actual physical deformation generating the pressure gradient.

In order to interpret our results on the fastest growing wavelength λ^* , we note that in dimensional terms the classical result for the flat substrate can be written as $\lambda_0^* \sim d^2 \sqrt{\sigma/A^*}$. One could expect the same general scaling to be valid for our case but with some effective film thickness and surface tension, d_{eff} and σ_{eff} . Increase in slip is equivalent to increasing d_{eff} and therefore leads to an increase in λ^* . Having an additional interface, on the other hand, is equivalent to a reduction of σ_{eff} .

To get a better picture of the relative significance of the two effects incorporated in our model, we plot the fastest growing wavelength of the instability as a function of the slip length in Fig. 3. While a range of values of β_0 between zero and 10 is investigated, the values of slip close to zero are not physically realistic since viscous effects in the air are not likely to result in such a dramatic reduction of slip at the interface. Remarkably, over a range of realistic values of β_0 , the wavelength λ^* is almost unchanged. Thus, the

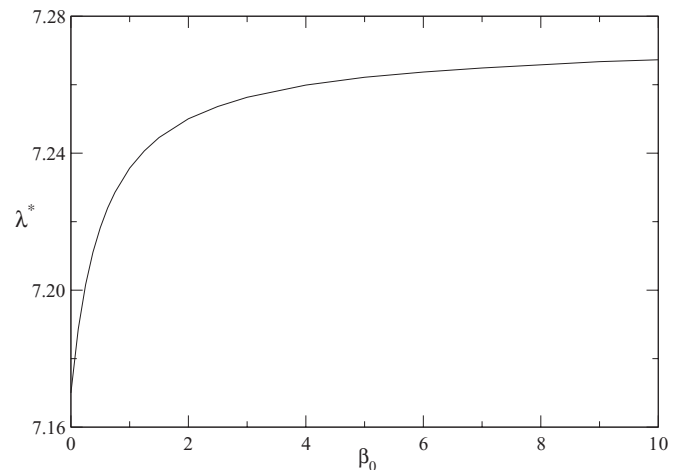


FIG. 3. The fastest growing wavelength of the instability as a function of the slip length in scaled coordinates for $L_c = 30$, $N_g = 15$, $w = l = 1$, $\varepsilon = 0.01$.

geometric effect of meniscus deformation and not the slip value is expected to be the key to wavelength selection. This is especially useful to note since getting accurate estimates of the actual slip length β_0 may be difficult without extensive numerical simulations of the air flow. The air is recirculating in the grooves due to the effects of the shear stress at the air-liquid menisci. Due to the very small size of the grooves, the effects of viscous stresses in the air are not negligible, which motivated the introduction of the finite slip length β_0 in our model. The general trend toward increasing the characteristic instability wavelength with an increase of the slip length is consistent with observations made from the numerical studies of slipping films on flat surfaces [20] and our argument from the previous paragraph. We also checked (for $\beta_0 = 10$) that the fastest growing wavelength increases as the groove width w decreases, which is to be expected since in the limit of small w the effect of the grooves should be negligible and the value of $\lambda^* = 2\sqrt{2\pi}$ corresponding to the flat substrate should be approached.

The effect of the structure in our formulation is modeled by a function $f(x)$ which involves an arbitrary small parameter ε . We verified that our conclusions, both here and below, are independent of the value of ε as long as it is of the order of 10^{-2} or below. For example, considering the parameter values listed in the caption to Fig. 3, we observed that reducing ε by a factor of two leads to the relative change of the growth rate on the order of 10^{-3} .

B. Film rupture

To investigate evolution of the film in the strongly nonlinear regime we carry out numerical simulations of Eq. (12) on the domain $[0, L_c]$ with N_g grooves and zero-slope and no-flux conditions at both endpoints. The spatial discretization method is the same as for the linear stability problem, except that a nonuniform mesh is introduced near the point of rupture, as discussed in more detail below. Time stepping is performed using the Gear's backward difference formula (BDF) method as implemented in the standard DVODE package. The value of L_c has to be large enough for instability, based on the linear stability theory from the previous subsection. As is common in rupture studies [13,22], we focus our attention on the minimum scaled film thickness a , which due to our choice of initial perturbation corresponds to $x = 0$. The result for $a \equiv h(0,t)/h(0,0)$ as a function of time is shown by the solid line in Fig. 4 for sinusoidal initial perturbation of amplitude 0.1 and wavelength $2L_c$. The dot-dashed line represents the result for flat substrate. Clearly, the rupture happens faster due to the effect of the structure, due to the same physical reasons as the increase in the growth rate of the small perturbations discussed in the previous subsection.

For steady lubrication-type flows near structured walls with grooves perpendicular to the direction of the flow, the effect of the grooves can be represented by an effective slip β_\perp^* , calculated, for example, in [19]. It may seem natural to expect the effect of the grooves in the present case to be represented by an effective slip. This, however, turns out to be not the case, for reasons which are twofold. First, the effective slip formula does not account for the menisci deformation in the grooves. Second, the flow is no longer steady, as was assumed

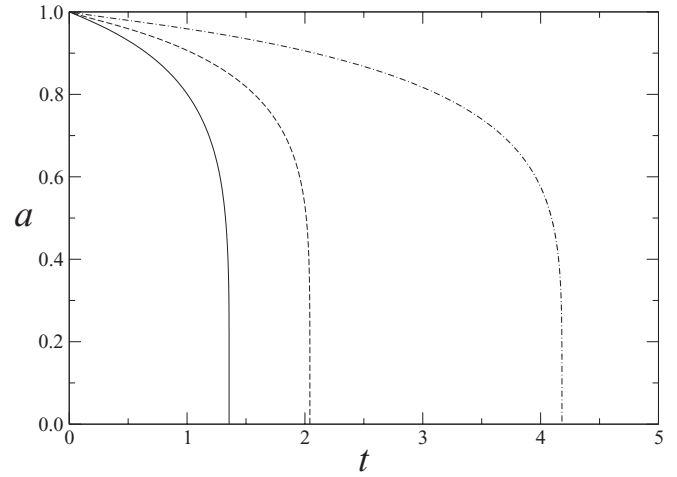


FIG. 4. Minimum scaled film thickness as a function of time for $L_c = 4$ found from different models: flat substrate with no slip (dot-dashed line), numerical calculation for structured surface with $w = l = 0.2$, $\varepsilon = 0.01$, $\beta_0 = 10$ (solid line); calculation based on effective slip (dashed line).

in deriving the formula for β_\perp^* . The result for rupture on a surface with uniform effective slip equal to β_\perp^* is shown in Fig. 4 by the dashed line; clearly, this approach overestimates the rupture time. It would be of interest to investigate whether an effective boundary condition of a different kind may be applicable to our situation, but such discussion is beyond the scope of the present paper.

The shapes of the deformed groove menisci can be obtained from our numerical solution for $h(x,t)$. By combining Eqs. (1) and (3),

$$h_{1xx} = -\frac{1}{2}(h_{xx} + p_g). \quad (17)$$

Integrating this equation twice in x , we obtain

$$h_1(x,t) = -\frac{1}{2}h(x,t) - \frac{1}{4}p_g x^2 + a_1 x + b_1, \quad (18)$$

where the constants a_1 and b_1 are determined by the pinning boundary conditions at the groove boundaries, $h_1(x_i,t) = h_1(x_i + w,t) = 0$ (with grooves numbered by $i = 1, \dots, N_g$). We note that the exact deformation of the interface depends on the relationship between p_g and the effective slip length, which can in principle be found from solving the Stokes flow equations in the gas phase, but doing so is beyond the scope of the present article. However, moderate variations of p_g do not dramatically alter the interface shapes, so we plot typical results using $p_g = 0$ in Fig. 5. This illustration provides an additional insight into why the effective slip models do not work well for the present situation: The deformation of the menisci is different in different parts of the film. This effect can be crucial for two-phase flows in microfluidic applications, but is not captured by the averaging techniques based on single phase flows. The pressure gradient is very large near the groove boundaries, effectively reducing the flow between segments corresponding to different grooves, but the pressure distributions away from the points x_i are similar to the ones for the case when the instability develops over a flat substrate.

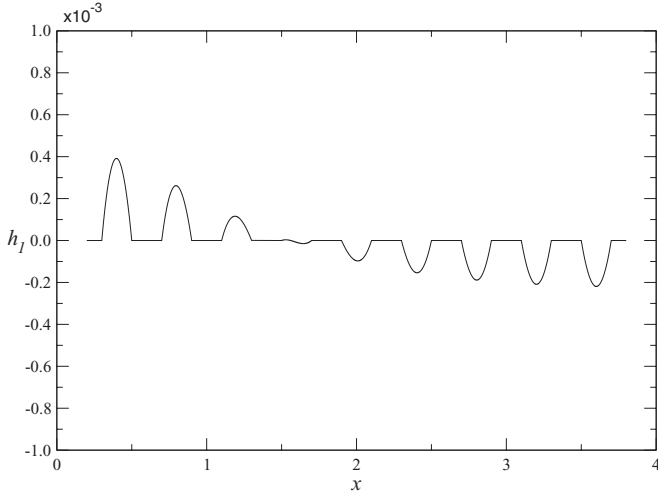


FIG. 5. Plot of the lower surface of the film at $t = 0.5$ for $p_g = 0$ showing deformed menisci in several grooves.

At the final stages of film rupture on a flat substrate with no-slip condition, the local solution near the rupture point is known to be self-similar [13], so that $a(t) \sim (t_R - t)^n$ with $n = 1/5$, where t_R is the rupture time. It has been suggested [20,22] that the introduction of slip at the bottom of the film changes the exponent to $n = 1/6$, but only moderately small values of a have been investigated in these previous studies. Here we carry out simulations over many orders of magnitude to verify the self-similarity, as shown in the plot in Fig. 6. Since $n = 1/6$ implies that $|a'(t)| \sim (t_R - t)^{-5/6}$, the log-log plot of $|a'(t)|$ versus a should be a straight line with the slope of -5 , which is indeed clearly seen in the figure (the dashed line of slope exactly equal to negative 5 is shown to illustrate our conclusion). The result shown in Fig. 6 also provides a verification of our numerical method. To achieve the accuracy needed for this calculation we used a nonuniform spatial mesh suggested by [13] (described in detail in the appendix to their paper) with second-order interpolation for the interface shape as the mesh changes, and a variable

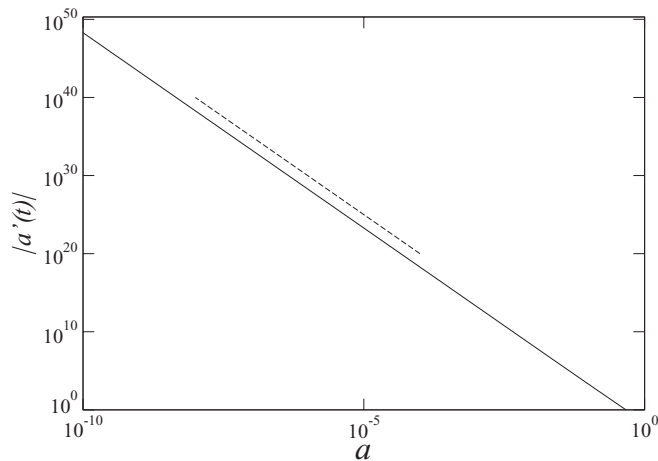


FIG. 6. A plot illustrating self-similar behavior at the final stages of rupture in the presence of slip for $\beta = 1$, $L_c = 4$. Dashed line has the slope of negative 5.

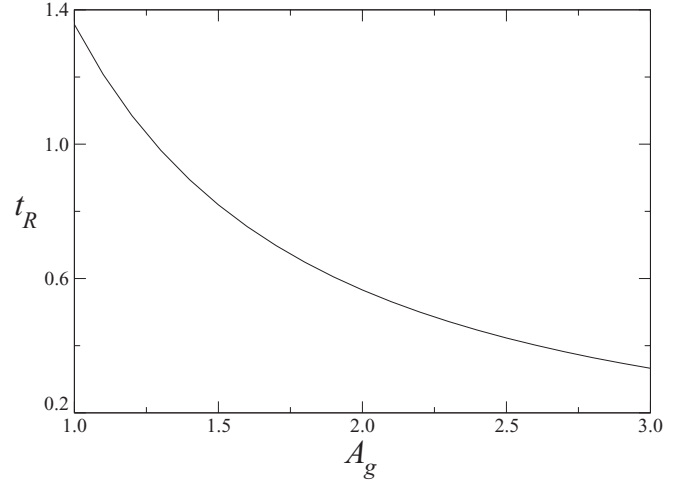


FIG. 7. Rupture time of the film as a function of the ratio of Hamaker constants for $\beta_0 = 10$, $N_g = 10$, $w = l = 0.2$.

time step proportional to a^6 , as suggested by the similarity solution.

IV. EFFECT OF VARIATIONS OF THE HAMAKER CONSTANT

The Hamaker constants are in general different for the parts of the film which are in contact with the solid phase and the gas phase. In the present model, this effect can be captured by choosing values of A_g different from s in Eq. (10). Let us first consider $s = 1$ and $A_g > 0$. Numerical simulations over a range of values of A_g indicate that in this case the film is unstable as long as the computational domain is chosen to be large enough. The total rupture time is shown as a function of A_g in Fig. 7. Estimating this time is important because even when the system is unstable, the value of rupture time in dimensional terms can be large compared to other time scales of interest for a particular application. Clearly, t_R decreases with an increase in the ratio of Hamaker constants, but at a slower rate for larger A_g .

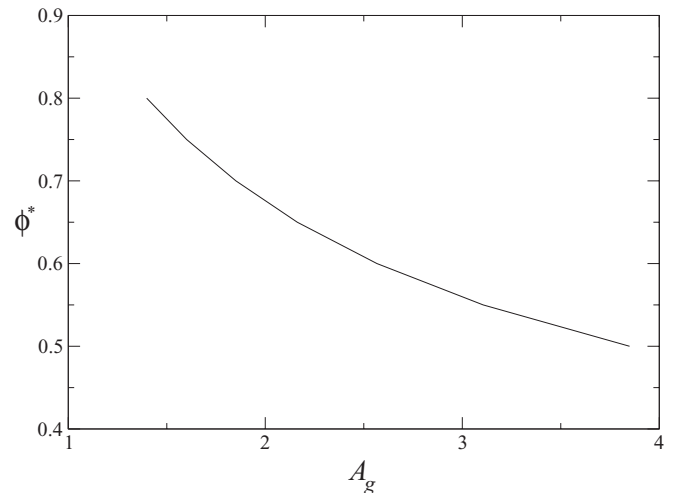


FIG. 8. The critical relative groove width $\phi = w/(w + l)$ as a function of the nondimensional Hamaker constant A_g .

A situation which can be encountered in applications is when the values of the Hamaker constant have different signs, with the one corresponding to the solid segment of the interface being negative. Based on the model of film on the flat substrate, one may expect stability. Let us investigate what happens when the effect of grooves is taken into account. Numerical simulations conducted for a range of values of β_0 indicate that the presence of the grooves can destabilize an otherwise stable film if their relative width, $\phi = w/(w + l)$, is large enough. The critical value of ϕ as a function of the ratio of Hamaker constants is shown in Fig. 8. The critical value is decreasing with the increase of the ratio of the Hamaker constants.

V. CONCLUSIONS

We formulated a mathematical model of rupture of a thin liquid film on a structured substrate. The general lubrication-type framework is similar to the previous studies of films on flat substrates, but three additional physical effects are introduced to account for the presence of the surface structure: spatial variations in the Hamaker constant, in the slip length, and deformation of the menisci separating air in the grooves from the liquid film. The value of the slip length at the menisci surfaces is assumed finite due to the effects of air viscosity.

For the case of negligible variations of the Hamaker constant, linear stability analysis of the uniform base state shows that the effect of surface structure is destabilizing. The scaled wavelength of the fastest growing mode of the linear theory is decreased compared to the classical value of $2\sqrt{2}\pi$. This prediction is in contrast to what is expected when the

structure is modeled by introducing an effective slip. The discrepancy is explained by the effect of the deformation of the menisci in the grooves. For a range of realistic values of the slip length, λ^* is found to be nearly independent from β_0 . Numerical simulations in the strongly nonlinear regime indicate that rupture time is decreased significantly due to the effect of the structure. Effective slip models tend to overestimate the rupture time. Thus, when a bubble is moving in a microchannel with a structured wall, the film separating the gas phase from the wall is likely to rupture faster than can be expected based on the classical theories of rupture (e.g., [12,13]) even if the effect of slip is incorporated into such theories. Self-similar rupture is observed at the final stages of evolution, with minimum film thickness decaying as $(t_R - t)^{1/6}$, where t_R is the rupture time.

Simulations are also conducted for the spatially nonuniform Hamaker constant. Rupture time is shown to decrease as the ratio of the maximum and minimum values of the Hamaker constant is increased. In addition, we showed that an otherwise stable film can be destabilized by the presence of sufficiently wide grooves and found the critical value of the groove size as a function of the parameters of disjoining pressure.

ACKNOWLEDGMENTS

This work was supported by the Ministry of Education and Science of the Russian Federation (Contract No. 02.740.11.5028) and by the US National Science Foundation Grant No. CBET-0854318. E.G. also acknowledges support from a grant of the President of the Russian Federation (Grant No. MK-240.2009.8).

-
- [1] L. Bocquet and J.-L. Barrat, *Soft Matter* **3**, 685 (2007).
 - [2] M. Sbragaglia and A. Prosperetti, *Phys. Fluids* **19**, 043603 (2007).
 - [3] A. V. Belyaev and O. I. Vinogradova, *J. Fluid Mech.* **652**, 489 (2010).
 - [4] A. Guenther and K. Jensen, *Lab Chip* **6**, 1487 (2006).
 - [5] V. S. Ajaev and G. M. Homsy, *Annu. Rev. Fluid Mech.* **38**, 277 (2006).
 - [6] A. Alexeev, T. Gambaryan-Roisman, and P. Stephan, *Phys. Fluids* **17**, 062106 (2005).
 - [7] D. V. Zaitsev, M. Lozano Aviles, H. Auracher, and O. A. Kabov, *Microgravity Sci. Technol.* **19**, 71 (2007).
 - [8] O. A. Kabov, *Thermophys. Aeromech.* **7**, 513 (2000).
 - [9] O. A. Kabov, D. V. Zaitsev, V. V. Cheverda, and A. Bar-Cohen, *Experimental Thermal and Fluid Science* **35**, 825 (2011).
 - [10] D. Quere, *Rep. Prog. Phys.* **68**, 2495 (2005).
 - [11] M. M. Williams and S. H. Davis, *J. Colloid Interface Sci.* **90**, 220 (1982).
 - [12] J. P. Burelbach, S. G. Bankoff, and S. H. Davis, *J. Fluid Mech.* **195**, 463 (1988).
 - [13] W. W. Zhang and J. R. Lister, *Phys. Fluids* **11**, 2454 (1999).
 - [14] R. Khanna, A. T. Jameel, and A. Sharma, *Ind. Eng. Chem. Res.* **35**, 3081 (1996).
 - [15] U. Thiele, L. Brusch, M. Bestehorn, and M. Bar, *Eur. Phys. J. E* **11**, 255 (2003).
 - [16] A. Sharma, R. Konnur, and K. Kargupta, *Physica A* **318**, 262 (2003).
 - [17] J. C.-T. Kao, A. A. Golovin, and S. H. Davis, *J. Colloid Interface Sci.* **303**, 532 (2006).
 - [18] E. Lauga, M. P. Brenner, and H. Stone, in *Handbook of Experimental Fluid Dynamics*, edited by C. Tropea, A. Yarin, and J. Foss, Chap. 15. (Springer, New-York, 2007).
 - [19] F. Feuillebois, M. Z. Bazant, and O. I. Vinogradova, *Phys. Rev. Lett.* **102**, 026001 (2009).
 - [20] K. Kargupta, A. Sharma, and R. Khanna, *Langmuir* **20**, 244 (2004).
 - [21] D. Peschka, A. Munch, and B. Niethammer, *Nonlinearity* **23**, 409 (2010).
 - [22] V. S. Ajaev, *Phys. Fluids* **18**, 068101 (2006).
 - [23] E. Ya. Gatapova and O. A. Kabov, *Microgravity Sci. Technol.* **19**, 132 (2007).
 - [24] R. V. Craster and O. Matar, *Rev. Mod. Phys.* **81**, 1131 (2009).
 - [25] A. Mazouchi and G. M. Homsy, *Phys. Fluids* **13**, 2751 (2001).
 - [26] R. Krechetnikov, *Phys. Fluids* **22**, 092102 (2010).
 - [27] V. S. Vladimirov, *Equations of Mathematics Physics* (Mir Publishers, Moscow, 1983).
 - [28] P. G. de Gennes, *Langmuir* **18**, 3413 (2002).